PAPER

A Target Shape Estimation Algorithm for Pulse Radar Systems Based on Boundary Scattering Transform

Takuya SAKAMOTO[†], ***Student Member and*** **Toru SATO**[†], ***Member***

SUMMARY Environment measurement is an important issue for various applications including household robots. Pulse radars are promising candidates in a near future. Estimating target shapes using waveform data, which we obtain by scanning an omni-directional antenna, is known as one of ill-posed inverse problems. Parametric methods such as Model-fitting method have problems concerning calculation time and stability. We propose a non-parametric algorithm for high-resolution estimation of target shapes in order to solve the problems of parametric algorithms.

key words: *pulse radar, non-parametric estimation, shape estimation, ill-posed inverse problem, boundary scattering transform*

1. Introduction

Environment measurement is an important issue for various applications including household robots. Pulse radar systems are promising candidates for environment measurement in a near future. FCC (Federal Communications Commission) has recently set a standard for ultra-wide-band (UWB) technologies. UWB pulse radars are attractive for this purpose.

Estimating target shapes using data received by a scanned omni-directional antenna is known as one of ill-posed inverse problems. Many kinds of imaging algorithms have been proposed [1]–[18]. Model fitting method is one of effective approaches for this problem [1], [2]. In the model fitting method, target shapes are expressed with parameters, and the parameters are updated to minimize the difference between the observed data and the estimated data. Model fitting method works well to some extent, but they have problems concerning calculation time and stability [3], [4]. Imaging algorithms based on domain integral equation is another parametric approach [5]–[13]. In their algorithm, targets and media were modeled as grids of permittivity. They solved domain integral equation by means of many kinds of optimization algorithms such as genetic algorithms. However, they assume that antenna scans around target, which is not realistic for our applications. Diffraction tomography is known as one of algorithms for radar imaging [14]. However, they also need to scan antenna at many locations around targets.

On the other hand, some non-parametric algorithms have been proposed. An estimation method of direction of arrival (DOA) based on focussing matrices has been proposed [15], [16]. Their algorithm deals with wide-band signals. However, they assume independent sources and plane waves, which are not valid for our problem. Furthermore, their purpose is to estimate only DOA, which is not sufficient. A source localization algorithm based on maximum-likelihood criterion has been proposed [17]. Their algorithm assumed near-field targets and wide-band signals. However, the locationing algorithm of point sources is not sufficient to target shape estimation. SRDI (Single-Range Doppler Interferometry) algorithm estimates space-debris rotating with single-range data for doppler radar systems [18]. SRDI assumes rotating targets, therefore it can not be applicable to our purpose. The conventional non-parametric algorithms have problems of unrealistic assumptions and insufficient performance for shape estimation.

We show the existence of a reversible transform between delay time and target shape in this paper. We call the transform IBST (Inverse Boundary Scattering Transform). We propose a non-parametric high-resolution shape estimation algorithm based on IBST. For the kind of problem dealt with in this paper, migration algorithms are well-known especially in the field of a seismic prospecting [19]. Migration algorithms are applicable for general media and targets, but their resolutions are limited to the order of the signal wavelength. The proposed algorithm using IBST has an advantage that it can uniquely and directly estimate target boundary shapes as lines, although IBST requires targets surrounded by smooth boundaries, uniform media and directly scattered waves.

Firstly, we prove the existence of a reversible transform between delay time and target shape in this paper. Next, we clarify problems in applying IBST to real data. We propose a selection algorithm and a false image reduction algorithm to solve the problems. Moreover, we propose an edge detection algorithm using IBST. Finally, we show application examples of IBST using a numerical experiment, and investigate the performance of the proposed algorithm.

2. System Model

We assume a mono-static radar system in this paper. An omni-directional antenna is scanned along a straight line. UWB pulses are transmitted at a fixed interval and received by the antenna. The received data is input into A/D converter, and stored into a memory. We estimate target shapes using the data.

We deal with a 2-dimensional problem, and TE-mode wave. Targets and the antenna are located on a plane. We

Manuscript received October 31, 2003.

[†]The authors are with the Department of Communications and Computer Engineering, Graduate School of Informatics, Kyoto University, Kyoto-shi, 606-8501 Japan.

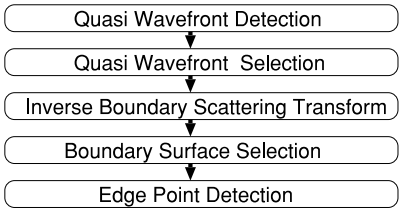

Fig. 1 Outline of the proposed algorithm.

define r-space as the real space, where targets and the antenna are located. If a set is expressed in r-space, we call it the expression in r-domain. We express r-space with the parameter (x, y). Both x and y are normalized by λ, which is the center wavelength of the transmitted pulse in a vacuum. We assume $y > 0$ for simplicity. The antenna is scanned along x-axis in r-space. We define $s'(X, Y)$ as the received electric field at the antenna location $(x, y) = (X, 0)$, where we define Y with time t and speed of the light c as $Y = ct/(2\lambda)$. We set $t = 0$ to the time which maximizes the instantaneous envelope of electric field at the location of the antenna. We apply a matched filter of transmitted waveform to $s'(X, Y)$. We define $s(X, Y)$ as the output of the filter. We define d-space as the space expressed by (X, Y). If a set is expressed in d-space, we call it an expression in d-domain. We normalize X and Y by λ and the center period of transmitted waveform, respectively.

We propose a non-parametric high-resolution estimation algorithm of target shape using the data $s(X, Y)$. Firstly, we extract quasi wavefronts, which is delay times of direct scattered waves. Next, we obtain approximate estimation of target shapes by applying IBST to the extracted quasi wavefronts. We then apply a selection algorithm and a false image reduction algorithm to the data by using evaluation value of target boundary based on the locations and shapes of targets. Finally, we estimate the target shapes and the edge-point locations. Figure 1 illustrates the outline of the algorithm we propose in this paper.

3. Boundary Scattering Transform and Its Inverse Transform

3.1 Boundary Scattering Transform

We prove the existence of a reversible transform between quasi wavefronts and target boundary surfaces in this section. Although we deal with a 2-dimensional problem, the algorithm can be easily extended to a 3-dimensional one. Additionally, we assume scanning of the antenna along a straight line, but it can be easily extended to scans along any curves.

We assume that each target has a uniform complex permittivity, and surrounded by a smooth boundary. The target complex permittivity of the target $\varepsilon(x, y)$ satisfies

$$|\nabla\varepsilon(x, y)|^2 = \sum_{q\in H} a_q \delta(y - g_q(x)), \tag{1}$$

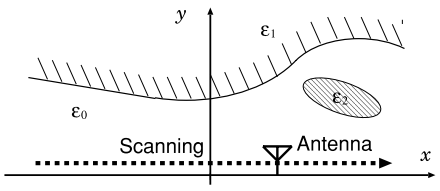

Fig. 2 The coordinates and an example of a target complex permittivity.

where δ is Dirac's delta function, and $g_q(x)$ is a differentiable single-valued function. We define

$$q = \{(x, y)|y = g_q(x), x \in J_q\} \in H, \tag{2}$$

where J_q is the domain of $g_q(x)$, a_q is a positive real constant which depend on $q \in H$, and H is the set of all q. We define target boundary surfaces as elements of H. Figure 2 illustrates the coordinates and an example of a target complex permittivity $\varepsilon(x, y)$ in r-space. The assumption of the target model in Eq. (1) is general because it includes the case where the target complex permittivity is divided into some areas as in Fig. 2.

Next, we define several sets in order to explain Boundary scattering transform. We define P, which is a subset of d-space, as

$$P = \{(X, Y)\,|\partial s(X, Y)/\partial Y = 0, |s(X, Y)| \geq T_s\}, \tag{3}$$

where T_s is a threshold to prevent picking up noise values.

Next, we connect the points close to each other in P. We obtain lines from P in this way. We express each line as p, which we call a quasi wavefront. We define G as the set of all $p \in P$.

Here, we assume that the medium of direct path is vacuum, but the following argument is valid for any uniform media only if the propagation speed of the wave is known. We assume p corresponds to the direct scattered wave of q. By utilizing the relationship between the antenna location and the length of perpendicular line to q from the antenna location, the point (X, Y) on p is expressed as

$$\begin{cases} X &= x + y\mathrm{d}y/\mathrm{d}x \\ Y &= y\sqrt{1 + (\mathrm{d}y/\mathrm{d}x)^2}, \end{cases} \tag{4}$$

where (x, y) is a point on q, and we assume $y > 0$ and $Y > 0$. We define the transform in Eq. (4) as Boundary Scattering Transform (BST).

Figure 3 shows an example of BST. The upper figure shows the target boundary surface in r-domain, and the lower figure is the corresponding quasi wavefront in d-domain, which is the BST of the upper figure. In general, some quasi wavefronts are generated from one target boundary surface by BST as in the figure.

3.2 Inverse Boundary Scattering Transform

If an inverse transform of BST exists, we can estimate target shapes using the transform. In this subsection, we prove the existence of the inverse transform of BST.

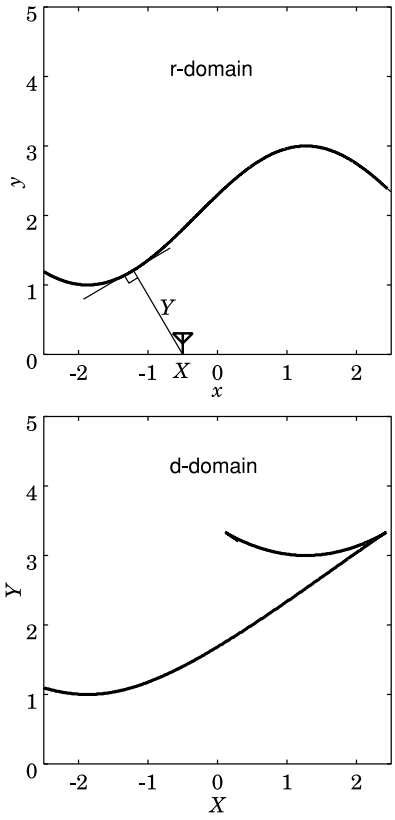

Fig. 3 An example of boundary scattering transform.

IBST is based on a back projection process. When there is a reflection at (X, Y) in d-space, the target is on a circle $C(x, y; X, Y)$ of its center $(X, 0)$ and its radius of Y in r-space. If a reflection forms a curve p, point (X, Y)'s on p produce a group of circles in r-space. The envelope of the group of circles must draw its target shape. This process is formulated as follows. Firstly, we express the circle for given (X, Y) using a point (x_c, y_c) on it. We define a group of circles $C(x_c, y_c; X, Y)$ as

$$\begin{aligned} &C(x_c, y_c; X, Y) \\ &\quad = \{(x_c, y_c) \,|\, y_c > 0, F_C(x_c, y_c; X, Y) = 0\}, \end{aligned} \tag{5}$$

where $F_C(x_c, y_c; X, Y)$ is expressed as

$$F_C(x_c, y_c; X, Y) = (x_c - X)^2 + y_c^2 - Y^2. \tag{6}$$

Next, we express the envelope of the group of circles $C(x_c, y_c; X, Y)$ using a point (x_e, y_e) on it. We define E_C as the envelope of the group of circles $C(x_c, y_c; X, Y)$. E_C satisfies

$$\begin{aligned} &E_C(x_e, y_e; X, Y) \\ &\quad = \{(x_e, y_e) \,|\, y_e > 0, F_C(x_e, y_e; X, Y) = 0, \\ &\qquad\qquad \partial F_C(x_e, y_e; X, Y)/\partial X = 0\}. \end{aligned} \tag{7}$$

Here, the partial derivative means the derivative independent only of x_e and y_e, not of Y. Here, we should note that Y is uniquely determined by X with a certain function. The equation of E_C is expressed as

$$\begin{cases} x_e &= X - Y\mathrm{d}Y/\mathrm{d}X \\ y_e &= Y\sqrt{1 - (\mathrm{d}Y/\mathrm{d}X)^2}. \end{cases} \tag{8}$$

We have to check if Eq. (8) works as an inverse transform of BST expressed in Eq. (4). Substituting Eq. (4) to Eq. (8), we obtain

$$y_e^2 - y^2 + (x_e - x)^2 - 2(x_e - x)y\mathrm{d}y/\mathrm{d}x = 0. \tag{9}$$

Equation (9) holds for any function $g_q(x)$, for any x. Therefore, we conclude that $x = x_e, y = y_e$. This means that Eq. (8) satisfies the condition of an inverse transform of BST. As a result, we conclude that the inverse transform of BST is given by

$$\begin{cases} x &= X - Y\mathrm{d}Y/\mathrm{d}X \\ y &= Y\sqrt{1 - (\mathrm{d}Y/\mathrm{d}X)^2}. \end{cases} \tag{10}$$

We define the transform in Eq. (10) as Inverse Boundary Scattering Transform (IBST). The existence of the inverse transform is very meaningful because it can be used for a direct and unique estimation of target boundary shapes. The estimated target boundaries are expressed as not an image but lines. This is the advantage and the characteristic of our algorithm.

The condition of existence of IBST is differentiability of the quasi wavefront and

$$|\mathrm{d}Y/\mathrm{d}X| \leq 1. \tag{11}$$

This inequality in Eq. (11) is required because if it is not satisfied, the value of y obtained using IBST in Eq. (10) is not a real number, which is not rational. In a situation of Fig. 2, a target perpendicular to x-axis produces a straight line of its inclination of 45 degrees in d-space. We assume that we can receive the directly scattered waves from the target boundary. However, if this condition is not satisfied, the estimation accuracies are degraded. Plural quasi wavefronts are generated from one target boundary surface by BST in general. However, if we find out all quasi wavefronts from the received data, it is possible to reconstruct the target boundary surfaces using IBST. Therefore, the plural quasi wavefronts generation has no problem in our algorithm.

3.3 Edge Refraction Waves and Boundary Scattering Transform

We have shown that the relationship between quasi wavefronts and target boundary surfaces is expressed as BST and IBST if the complex permittivity satisfies the condition in Eq. (1). If IBST is applicable not only for reflection but also for refraction, we see that IBST has a great deal of application range. In this subsection, we investigate the relationship between edge refraction waves and IBST.

If an edge point of a target is located at (α, β), the delay time of received signal is expressed as a hyperbola as

$$Y = \sqrt{(X - \alpha)^2 + \beta^2}. \tag{12}$$

The IBST of Eq. (12) is $[x, y]^{\mathrm{T}} = [\alpha, \beta]^{\mathrm{T}}$, where T means transpose. BST of the edge point is not defined because the differentiability condition is not satisfied in this case. However, it is possible to estimate the edge point location using IBST. Substituting the hyperbola in Eq. (12) to BST in Eq. (4), we obtain the differential equation expressed as

$$\mathrm{d}y/\mathrm{d}x = (y^2 - x^2 - \beta^2)/2xy, \tag{13}$$

where we assume $\alpha = 0$ because α works only as a parallel translation of x. If the solution of Eq. (13) draws a certain curve, it brings a trouble in applying IBST, because it means that a target boundary surface exists which has the same quasi wavefront of an edge point. Therefore, it is important to investigate a differential equation of Eq. (13), which is one of Bernoulli-Riccati differential equations. Considering $y \geq 0$, the general solution of the equation is expressed as

$$y = \sqrt{\beta^2 - x^2 - Cx}, \tag{14}$$

where C is an integral constant. The BST of Eq. (14) is expressed as

$$[X, Y]^{\mathrm{T}} = \left[-C/2,\ \sqrt{C^2/4 + \beta^2}\right]^{\mathrm{T}}. \tag{15}$$

The solution of the differential equation expresses a circle with a radius $\sqrt{\beta^2 + C^2/4}$, and center $[-C/2, 0]^{\mathrm{T}}$. The BST of Eq. (15) shrinks to a point on the hyperbola in Eq. (12). The differential of a point is not defined, therefore it has no problem in applying IBST to data.

Consequently, IBST is applicable to both of reflection waves and refraction waves. IBST precisely estimates target boundary surfaces and edge point locations if an antenna can receive the directly scattered waves from the target boundary. We propose the algorithm using IBST in this paper, and show an example of application of IBST in the following sections.

4. Quasi Wavefront Extraction from Received Data

4.1 Extraction of Quasi Wavefront

In this section, we describe the method of extraction of quasi wavefronts. We have already defined the set P. The procedure of extraction of P is easy because all we should do is to check the derivative of given data. Next, we go on to the procedure of extracting $p \in G$ from P. In an actual procedure, we sequentially connect the points in P which satisfy a required condition. $p \subset P$ are connected closed sets. The i-th set p_i is determined as follows. The first element of p_i is an arbitrary element of P which is not included in $p_1, p_2, \cdots, p_{i-1}$. The domain I_i for p_i is set to X of the first element. The second element of p_i is chosen from P which satisfies $|\mathrm{d}Y/\mathrm{d}X| \leq 1$ in Eq. (11). Here, Y should have only one value for the same X. Then, domain I_i is updated according to the newly chosen element. In this way, we expand the set p_i until there is no other element which can be included into p_i. Finally, the extracted p_i has a characteristic as

$$p_i = \{(X, Y) | Y = f_i(X), |\mathrm{d}f_i(X)/\mathrm{d}X| \leq 1, X \in I_i\}, \tag{16}$$

where $f_i(X)$ is a single-valued function whose domain is I_i. Eq. (16) means that a unique Y has to exist satisfying $(X, Y) \in p_i$ for any $X \in I_i$. The algorithm described in the next subsection removes the undesirable links generated in this procedure.

4.2 Evaluation of Quasi Wavefront

As mentioned in the previous section, $p \in G$ denote quasi wavefronts which correspond to direct scattered waves from targets. Simply extracted quasi wavefronts include false quasi wavefronts generated by noises, ringing of waveforms, and multiple scattering. It is important to remove these false quasi wavefronts.

We define an evaluation value w_i for $p_i \in G$ as

$$w_i = \left| \int_{X \in I_i} s(X, f_i(X)) \mathrm{d}X \right|^2. \tag{17}$$

w_i becomes large when both of the amplitude of the signal along the quasi wavefront, and the width of the domain of $f_i(X)$ are large. If both of positive and negative points exist in a quasi wavefront, the evaluation value becomes small. This characteristic is valid because quasi wavefront should be constructed by connecting points with same phases. Figure 4 illustrates the reason why we adopt the integration of the signal amplitude as an evaluation value. If we adopt the integration of the signal power as an evaluation value, undesirable quasi wavefronts are extracted as shown in the right panel of Fig. 4.

We can remove false quasi wavefronts caused by noises and ringing of waveforms by utilizing the evaluation value w_i for most cases. However, the evaluation value for a false quasi wavefront becomes large when the false quasi wavefront is close to real quasi wavefronts. In this case, the evaluation value in Eq. (17) is not sufficient. In order to solve this problem, we propose the following algorithm which allows us to subdivide the regions. The procedure described in Sec. 4.1 does not exclude situations that $p_1 \cap p_2 \neq \phi$(nullset) for $p_1, p_2 \in G$, $p_1 \neq p_2$ as shown in Fig. 5. In such a case we subdivide the quasi wavefront so that the two sets contain only one element in common. In the figure, $p_1 = \{a, b, e, f, g\}$ and $p_2 = \{a, b, c, d\}$. In this case, we divide the quasi wavefront as $p_1 \rightarrow p_1'$ if $w_{p_1} \leq w_{p_2}$. Note that p_1' has lower evaluation value than p_1. If $w_{p_1} \geq w_{p_2}$ holds,

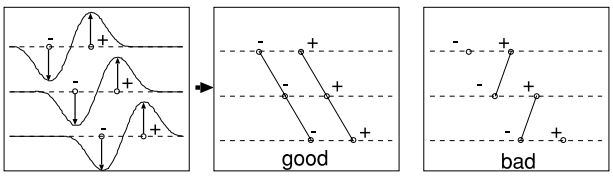

Fig. 4 Amplitude and quasi wavefronts.

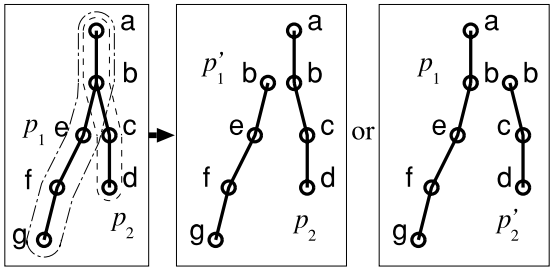

Fig. 5 Outline of division algorithm for quasi wavefronts.

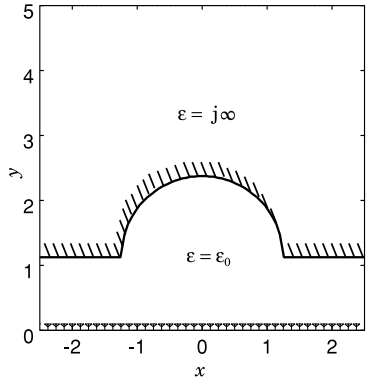

Fig. 6 The target boundary surface used for the application example.

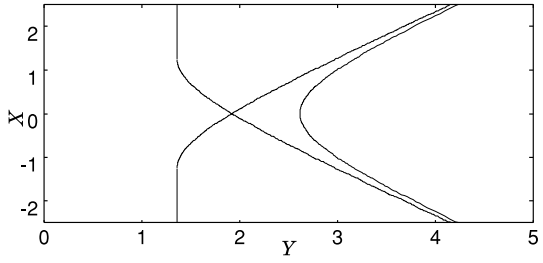

Fig. 7 BST of the target boundary surface in Fig. 6.

we divide p_2 as $p_2 \to p_2'$. Here, $p_1' \cup p_2 = p_1 \cup p_2' = p_1 \cup p_2$, $p_1' \cap p_2 = p_1 \cap p_2'$ and $|p_1' \cap p_2| = |p_1 \cap p_2'| = 1$ are satisfied, where $|p|$ represents the number of elements of the set p. In Fig. 5, $p_1' \cap p_2 = p_1 \cap p_2' = \{b\}$. After this subdivision, we can remove regions with small w_i by recalculating w_i.

4.3 An Example of Application of Quasi Wavefronts Extraction

We show an example of application of the extraction algorithm of quasi wavefront, which we explained in the previous subsection. Figure 6 shows an example of target boundary surface. The upper domain in the figure is filled with perfect electric conductor, and the lower domain is filled with air. The symbols located at the bottom of the figure show the locations of the antenna, where we receive signals. Figure 7 shows the BST of the target in Fig. 6. We calculate refraction waves from the edge points in another way, because we can not derive it using BST. In the figure, plural quasi wavefronts are generated. Extraction of these true quasi wavefronts enable us to estimate the target shape using IBST.

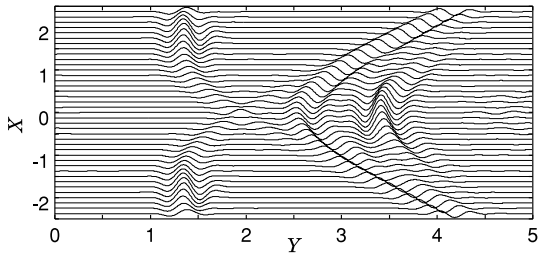

Fig. 8 An example of received signal $s(X, Y)$.

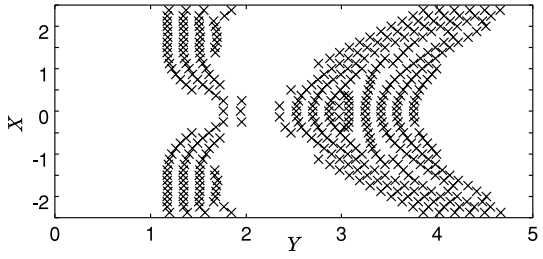

Fig. 9 Extraction of set P from data $s(X, Y)$.

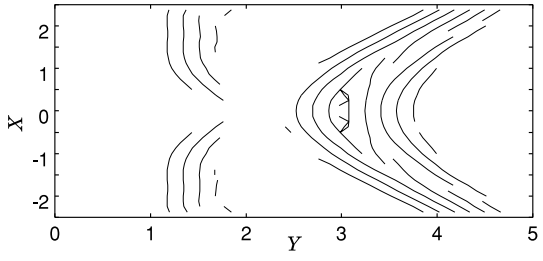

Fig. 10 Extraction of quasi wavefront $p \in G$ from data $s(X, Y)$.

Figure 8 shows the received data from the target shown in Fig. 6, which we obtain by utilizing FDTD (Finite Difference Time Domain) method. We receive the signal at the 40 locations illustrated in Fig. 6, whose intervals are 0.0125λ. Here, we assume a noiseless case. There is a false quasi wavefront caused by multiple scattering in the figure. Except for it, other quasi wavefronts are approximately same in Fig. 7. Figure 9 shows a set P extracted from the signal in Fig. 8. We select the points in d-domain where the differential of the waveform is equal to zero. Here, we remove points with small power by a ranking algorithm. Numerous undesired points exist in P due to the ringing of the waveform. Figure 10 shows $\cup_{p \in G} p$, which is the set of all quasi wavefronts p extracted from the received signal. As mentioned above, quasi wavefronts $p \in P$ satisfies $|\mathrm{d}Y/\mathrm{d}X| \leq 1$, which is the condition of existence of IBST.

Our algorithm extract quasi wavefronts at large, and they include a part of edge refraction wave shown in Fig. 7, because we utilize a ranking algorithm in extraction of P. On the other hand, undesired quasi wavefronts and multiple scattering waves also appear. We apply the quasi wave-

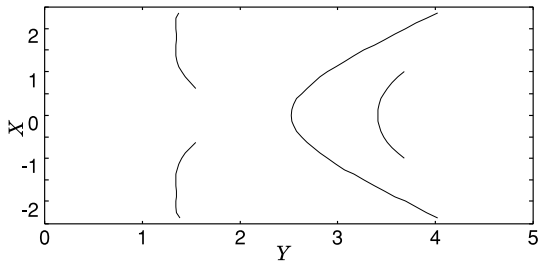

Fig. 11 Selection of quasi wavefronts using evaluation values.

front division algorithm to $p \in G$ based on the evaluation values as explained in the previous subsection, and then we recalculate the evaluation values for updated quasi wavefronts. Next, we select the quasi wavefront whose evaluation value is greater than $-n$ dB of the maximum evaluation value. Figure 11 shows the updated and selected quasi wavefronts, where an empirically chosen value of $n = 10$ is used. The proposed algorithm above extracts 4 quasi wavefronts from the received signal. These are approximately equal to the real quasi wavefronts in Fig. 7 except for the false quasi wavefront caused by the multiple scattering. Although the proposed algorithm extract only a part of the edge refraction quasi wavefronts, it is sufficient for locationing of edge points.

5. False Image Reduction for Multiple Scattering and Edge Point Locationing

5.1 An Example of Application of IBST

Here, we show an example of the application of IBST. We apply IBST to the quasi wavefronts in Fig. 11. We utilize a smoothing algorithm with B-spline function in order to obtain the differential of a quasi wavefront. Figure 12 shows a result of IBST application. The solid line and the broken line in the figure are the real target boundary surface and the estimated target boundary surface respectively. The target shape is estimated by IBST in the figure. However, a false image appears above the real target. This is caused by the multiple scattering, and it is difficult to remove the false image in the algorithm of quasi wavefront extraction as described above.

5.2 False Image Reduction Algorithm for Multiple Scattering

In this subsection, we propose an algorithm which removes the false image caused by multiple scattering. We see that the false image is behind the true target boundary from the antenna position. We can remove the false image by using this nature. Firstly, we assume a segment between a point of an estimated target boundary and the antenna position where we receive the directly scattered waveform from the point. If other estimated target boundaries exist near the segment, the reliability of the estimated target boundary is reduced because the received power from the point is reduced by the

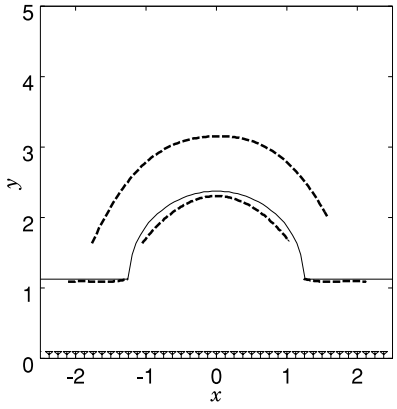

Fig. 12 An example of application of IBST.

obstacle target between the target and the antenna. Therefore, we reduce the evaluation value for the target boundary in that case. We also utilize the evaluation value of the obstacle targets for the penalty value. We formulate this process as follows.

We define a domain F_p using X satisfying $(X, Y) \in p$ and x, y satisfying $(x, y) \in \mathcal{B}^{-1}[p]$ as

$$F_p = \left\{ (x_0, y_0) \,\middle|\, \sqrt{(x-x_0)^2 + (y-y_0)^2} + \sqrt{(X-x_0)^2 + y_0^2} - \sqrt{(x-X)^2 + y^2} < 1/2 \right\}, \tag{18}$$

which is known as the 1st Fresnel zone. Here, we define $\mathcal{B}$ as the BST operator. We propose an algorithm which update the evaluation value w_i to the new evaluation value W_i as

$$W_i = w_i - \sum_{p_j \neq p_i \in G} w_{p_j} R_{p_j, p_i} \tag{19}$$

where $R_{r,p}$ means the ratio of the length of a quasi wavefront r whose BST is within F_p to the total length of r. The 2nd term of the right hand side of Eq. (19) means the penalty value for the evaluation value. The evaluation value W_i becomes small when other targets are in its 1st Fresnel zone. We utilize not a segment but 1st Fresnel zone for the algorithm because any other objects in the 1st Fresnel zone may significantly reduce the power of the received signal. Figure 13 shows the estimated target boundary surfaces using the new evaluation value W_i. The solid line and the broken lines are the real target boundary surface and the estimated target boundary surfaces, respectively. Here, we select the target boundary surface whose evaluation value is larger than $-n$ dB of the maximum evaluation value. Here we use an empirically chosen value of $n = 10$. The proposed algorithm successfully removes the false image of the boundary surface. The degradation of the estimation accuracy on the concave surface compared to the straight surface is caused by the difference between the observed waveform and the reference waveform for the matched filter. The target shape estimation accuracy is approximately 0.1 λ at most.

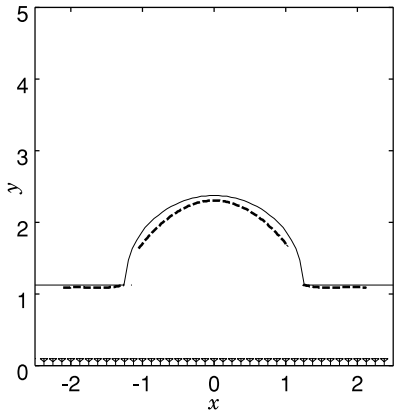

Fig. 13 The estimated target shape by false image reduction algorithm.

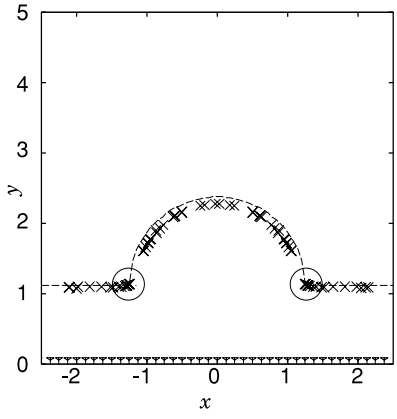

Fig. 14 The target boundary surfaces sampled at non-equi-interval and the detected edge points.

5.3 Edge Point Locationing Algorithm

We obtain the target boundary surface sampled at non-equi-intervals if we apply IBST to the quasi wavefronts sampled at equi-interval of X in d-domain. Figure 14 shows an example of the target boundary surface sampled at non-equi-interval. The solid line is the real target boundary surface, and the cross symbols are the target boundary surfaces. It is possible to detect edge points using IBST because IBST concentrates a quasi wavefront from an edge point to a single point. We propose an edge point locationing algorithm as follows.

Firstly, we count the number of the points within the circle with a radius d and the center which is equal to each point of an estimated boundary. We call the number of the points the evaluation value for the point. Then, we search the point which maximizes the evaluation value. The found point is considered as an edge point. Next, we search the same way on the condition that the search area is limited to the field which is not within the circles with a radius d and the center which is equal to the found edges so far. This procedure is repeated. We adopt the detected edge points whose evaluation values are larger than $-n$ dB of the maximum evaluation value.

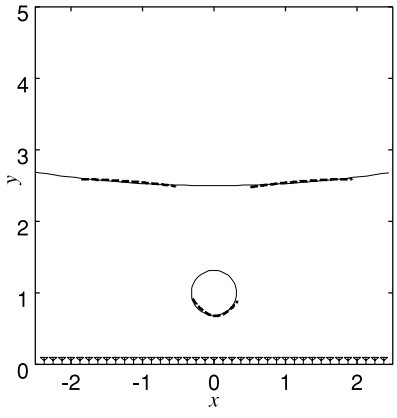

Fig. 15 An application example of IBST for a target boundary with an obstacle cylinder.

We apply the algorithm for edge points detection mentioned above. Here we use an empirically chosen parameters of $d = 0.2\lambda$, and $n = 10$. The two circle symbols in Fig. 14 show the detected edge points. The both edge locations are estimated accurately.

5.4 The Application Limitation of IBST

In this subsection, we examine the application limitation of IBST. Firstly, we consider a case that we do not obtain a directly scattered wave from a part of target. We show an application example of IBST for a curved target with a cylinder in its foreground. In Fig. 15 the solid line and the broken line show the true boundary and the estimated boundary, respectively. We see in the figure that IBST cannot reconstruct the part of the target behind the other object. Additionally, the upper part of the cylinder is not estimated either. In this way, the part of targets without directly scattered wave cannot be estimated by our algorithm.

Next, we explain another limitation of IBST. If the target is a circle whose center is on the scanning line of the antenna, the directly scattered waves shrink to only one point in d-space, which we mentioned in section 3. In this case, we can not estimate the boundary with the extraction algorithm of quasi wavefronts. We may deal with this problem by searching an isolated point with large power. In this case, we should distinguish the peaks caused by circle-shaped surfaces from peaks caused by noises. In anyway, further studies are required to solve the problem.

6. Performance against Noise

We investigate the performance of the proposed algorithm in a noisy environment. Figure 16 shows the raw received signal $s'(X, Y)$ for S/N = 3 dB. Figure 17 shows $s(X, Y)$, which is the output signal of a matched filter for the raw signal in Fig. 16. The signal power is not uniquely defined because the signal is not stationary. Here, we define S as

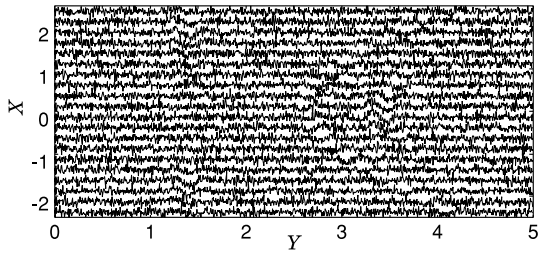

Fig. 16 A raw signal $s'(X, Y)$ for S/N = 3 dB.

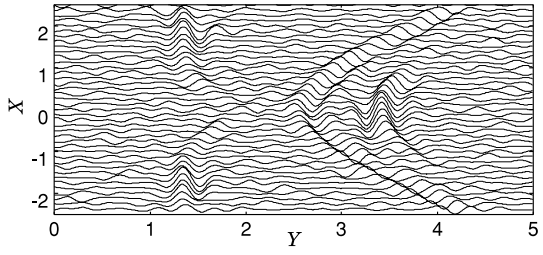

Fig. 17 A received signal $s(X, Y)$ for S/N = 3 dB.

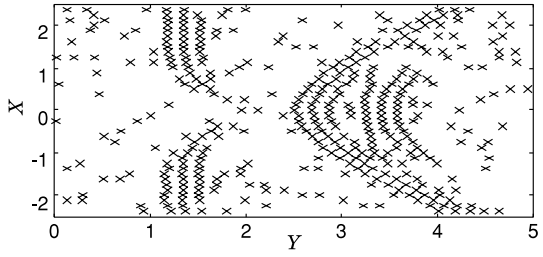

Fig. 18 Extraction of set P from data $s(X, Y)$ for S/N = 3 dB.

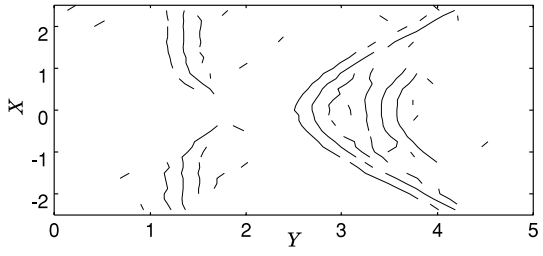

Fig. 19 Extraction of quasi wavefront p ∈ G from data $s(X, Y)$ for S/N = 3 dB.

$$S = \frac{1}{X_{\max} - X_{\min}} \int_{X_{\min}}^{X_{\max}} \max_{Y} |s(X, Y)|^2 \, \mathrm{d}X. \tag{20}$$

This definition utilizes the average of a maximum instantaneous power for each antenna location as the signal power.

Figure 18 shows the extracted set P from $s(X, Y)$ in Fig. 17 using the proposed algorithm. Many undesired points appear in the figure compared to that in Fig. 9. Figure 19 shows $\cup_{p \in G} p$, which is the set of all quasi wavefronts. Most of undesired points in Fig. 18 disappear because they do not satisfy the condition $|\mathrm{d}Y/\mathrm{d}X| \leq 1$. Therefore, meaningful quasi wavefronts are extracted by our algorithm. However, some residual undesired quasi wavefronts

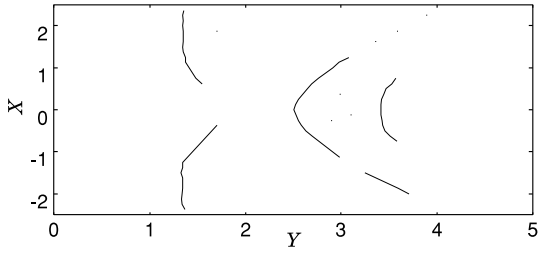

Fig. 20 Selection of quasi wavefronts using evaluation values for S/N = 3 dB.

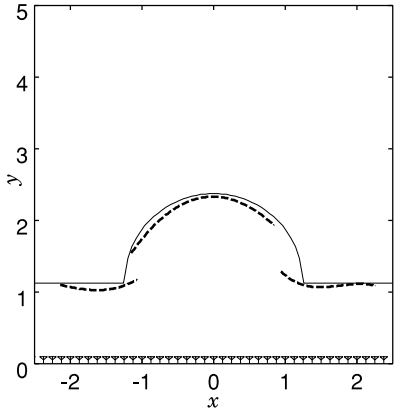

Fig. 21 The estimated target shape for S/N = 3 dB.

remain in the figure. Next, we apply our selection algorithm using evaluation value in Eq. (17) to $p \in G$ in Fig. 19. Figure 20 shows the selected quasi wavefronts by our selection algorithm. The extracted quasi wavefronts in the figure are slightly different from those in Fig. 11. They are distorted by noise, and a part of the quasi wavefront from the concave surface disappears in the figure. However, all desired quasi wavefronts are correctly extracted by the proposed algorithm.

Figure 21 shows the estimated target shape by applying IBST and multiple scattering reduction algorithm to the extracted quasi wavefronts in Fig. 20. Although the estimated target shape in Fig. 21 is inferior to Fig. 13, the outline of the target shape is estimated successfully. Consequently, the proposed algorithm has a robustness even for a poor S/N such as 3 dB.

7. Conclusion

We proposed a non-parametric algorithm of estimating target shapes for UWB pulse radar systems. We clarified the existence of a reversible transform between a target shape and a delay time image, which we call BST and IBST. The proposed algorithm makes use of the transform and achieves a high resolution imaging.

Firstly, we extracted quasi wavefronts from a received signal. We proposed quasi wavefront extraction, division, and selection algorithms using an evaluation value, which remove undesirable quasi wavefronts caused by noise and

ringings. Next, we applied IBST to the data to estimate the target shapes. The target shape estimation using IBST have a remarkable performance. Moreover, we proposed a false image reduction algorithm caused by multiple scattering. We have shown that the algorithm removed the false images completely. In addition, we proposed an edge locationing algorithm using IBST, and showed an application example. We clarified that the estimation accuracy is 0.1 wavelength in the worst case. We also investigated the performance of the proposed algorithm in a noisy environment. The proposed algorithm has a good performance for S/N=3 dB. The achieved accuracy is sufficient for most of applications.

Acknowledgment

This work is supported in part by the 21st Century COE Program (Grant No. 4213201).

References

[1] J.V. Candy and C. Pichot, "Active microwave imaging: A model-based approach," IEEE Trans. Antennas Propag., vol.39, no.3, pp.285–290, 1991.
[2] P. Chaturvedi and R.G. Plumb, "Electromagnetic imaging of underground targets using constrained optimization," IEEE Trans. Geosci. Remote Sens., vol.33, no.3, pp.551–561, 1995.
[3] T. Sato, K. Takeda, T. Nagamatsu, T. Wakayama, I. Kimura, and T. Shinbo, "Automatic signal processing of front monitor radar for tunnelling machines," IEEE Trans. Geosci. Remote Sens., vol.35, no.2, pp.354–359, 1997.
[4] T. Sato, T. Wakayama, and K. Takemura, "An imaging algorithm of objects embedded in a lossy dispersive medium for subsurface radar data processing," IEEE Trans. Geosci. Remote Sens., vol.38, no.1, pp.296–303, 2000.
[5] W.C. Chew and Y.M. Wang, "Reconstruction of two dimensional permittivity distribution using the distorted Born iterative method," IEEE Trans. Med. Imaging, vol.9, no.2, pp.218–225, 1990.
[6] M. Moghaddam and W.C. Chew, "Study of some practical issues in inversion with the Born iterative method using time-domain data," IEEE Trans. Antennas Propag., vol.41, no.2, pp.177–184, 1993.
[7] G.P. Otto and W.C. Chew, "Microwave inverse scattering—Local shape function imaging for improved resolution of strong scatterers," IEEE Trans. Microw. Theory Tech., vol.42, no.1, pp.137–142, 1994.
[8] H. Harada, D. Wall, T. Takenaka, and M. Tanaka, "Conjugate gradient method applied to inverse scattering problem," IEEE Trans. Antennas Propag., vol.43, no.8, pp.784–792, 1995.
[9] A.E. Yagle and J.L. Frolik, "On the feasibility of impulse reflection response data for the two-dimensional inverse scattering problem," IEEE Trans. Antennas Propag., vol.44, no.12, pp.1551–1564, 1996.
[10] A. Franchois and C. Pichot, "Microwave imaging—Complex permittivity reconstruction with a levenberg-marquardt method," IEEE Trans. Antennas Propag., vol.45, no.2, pp.203–215, 1997.
[11] C. Chiu and W. Chen, "Electromagnetic imaging for an imperfectly conducting cylinder by the genetic algorithm," IEEE Trans. Microw. Theory Tech., vol.48, no.11, pp.1901–1905, 2000.
[12] T. Takenaka, H. Jia, and T. Tanaka, "Microwave imaging of an anisotropic cylindrical object by a forward-backward time-stepping method," IEICE Trans. Electron., vol.E84-C, no.12, pp.1910–1916, Dec. 2001.
[13] C. Chiu, C. Li, and W. Chan, "Image reconstruction of a buried conductor by the genetic algorithm," IEICE Trans. Electron., vol.E84-C, no.12, pp.1946–1951, Dec. 2001.
[14] D. Nahamoo, S.X. Pan, and A.C. Kak, "Synthetic aparture diffraction tomography and its interpolation-free computer implementation," IEEE Trans. Sonics Ultrason., vol.31, no.4, pp.218–229, 1984.
[15] H. Hung and M. Kaveh, "Focussing matrices for coherent signal-subspace processing," IEEE Trans. Acoust., Speech Signal Process., vol.36, no.8, pp.1272–1282, 1988.
[16] S. Sivanand, J. Yang, and M. Kaveh, "Focusing filters for wide-band direction finding," IEEE Trans. Signal Process., vol.39, no.2, pp.437–445, 1991.
[17] J.C. Chen, R.E. Hudson, and K. Yao, "Maximum-likelihood source localization and unknown sensor location estimation for wideband signals in the near-field," IEEE Trans. Signal Process., vol.50, no.8, pp.1843–1854, 2002.
[18] T. Sato, "Shape estimation of space debris using single-range doppler interferometry," IEEE Trans. Geosci. Remote Sens., vol.37, no.2, pp.1000–1005, 1999.
[19] M.B. Dobrin and C.H. Savit, Introduction to Geophysical Prospecting, Fourth ed., McGraw-Hill, New York, 1988.

Takuya Sakamoto received the B.E. degree from Kyoto University in 2000, the M.I. degree from Graduate School of Informatics, Kyoto University in 2002. He is currently studying for the Ph.D. degree at Graduate School of Informatics, Kyoto University. His current research interest is in digital signal processing. He is a member of the IEEJ.

Toru Sato received his B.E., M.E., and Ph.D. degrees in electrical engineering from Kyoto University, Kyoto, Japan in 1976, 1978, and 1982, respectively. He has been with Kyoto University since 1983 and is currently a Professor in the Department of Communications and Computer Engineering, Graduate School of Informatics. His major research interests have been system design and signal processing aspects of atmospheric radars, radar remote sensing of the atmosphere, observations of precipitation using radar and satellite signals, radar observation of space debris, and signal processing for subsurface radar signals. Dr. Sato was awarded Tanakadate Prize in 1986. He is a member of the Society of Geomagnetism and Earth, Planetary and Space Sciences, the Japan Society for Aeronautical and Space Sciences, the Institute of Electrical and Electronics Engineers, and the American Meteorological Society.